Available online at www.sciencedirect.com

SCIENCE DIRECT®

Composites: Part A 35 (2004) 605–616

composites
Part A: applied science and manufacturing

www.elsevier.com/locate/compositesa

Low-velocity impact behaviour of fibreglass–aluminium laminates

G. Caprino[a,*], G. Spataro[b], S. Del Luongo[a]

[a]*Department of Materials and Production Engineering, University of Naples "Federico II", Piazzale Tecchio 80, 80125 Naples, Italy*
[b]*Alenia Aerospazio S.p.A., Viale dell'Aeronautica, 80038 Pomigliano d'Arco, Italy*

Received 17 July 2003; revised 22 October 2003; accepted 6 November 2003

Abstract

Low-velocity impact tests were performed on fibreglass–aluminium composites made of 2024 T3 sheets and S2-glass/epoxy prepreg layers, using an instrumented falling weight machine. For comparison purposes, similar tests were carried out on monolithic 2024 T3 sheets of equivalent thickness. In the tests, the impact speed, mass, and energy were varied, to ascertain the influence of these parameters on the material response. From the results obtained, the overall force–displacement curve only depends on the impact energy, rather than on the mass and speed separately. Further, the energy required for penetration is higher for monolithic aluminium than for the fibreglass–aluminium. However, the latter material seems to offer better performance than carbon fibre- and glass fibre-reinforced laminates in terms of penetration energy, damage resistance, and inspectability. The main failure modes of fibreglass–aluminium were assessed by both ultrasonic C-scan and chemical grinding of aluminium sheets. It was found that the energy required for first failure is very low, whereas the energy level resulting in first fibre failure is similar to that inducing first cracking in the 2024 T3 sheets. From the experimental data, simple empirical relationships were found for the calculation of maximum contact force, energy, and residual displacement as a function of the maximum displacement.

Keywords: A. Hybrid; B. Impact behaviour; B. Delamination; D. Ultrasonics; Mechanical testing

1. Introduction

In the last decades, the requirement of the aeronautical industry for a reduction in aeroplane life-cycle costs has driven the research towards new materials and fabrication methods, allowing cheaper component production, longer inspection intervals, and lower fuel consumption. Undoubtedly, the introduction of carbon fibre-reinforced plastics (CFRPs) instead of aluminium alloys has induced interesting weight savings, favourably affecting fuel costs. Further, the good fatigue behaviour of composites is lowering the maintenance costs. On the other hand, these advantages have been partially balanced by an increase in fabrication costs, deriving from the labour-intensive lay-up process, whereas the susceptibility of laminates to impact damage does not permit yet the full exploitation of their potentialities.

A multiplicity of routes, going from the utilisation of computer numerically controlled machines for automatic fibre placement [1,2] to stitching and Z-pinning [3,4] coupled with resin film infusion, have been undertaken to resort to cost-effective composite structures characterised by slow crack growth rates in fatigue and high impact damage resistance and tolerance. However, from the material side, about 15 years ago a new class of materials, made of alternating metallic and fibre-reinforced plastic (FRP) layers and generally known as 'fibre–metal laminates' (FMLs), was proposed [5]. The most popular FML among those commercially available is GLARE®, in which 2024 T3 aluminium alloy is used as metallic sheets and S2-glass/epoxy as FRP layers. GLARE® is adopted in the C-17 aft cargo door, but a more demanding primary application presently under evaluation is the pressurised fuselage of Airbus 340 and A3XX [5].

The basic scope in developing FMLs was to combine the good fatigue behaviour of FRPs with the excellent impact resistance of metals. In fact, enough experimental data have been generated, demonstrating the superior fatigue performance of GLARE® compared to monolithic aluminium alloys [6,7]. Some evidence has also been given that FMLs behave better than FRPs under impact conditions [8,9]. However, the mechanisms of damage development under

* Corresponding author. Tel.: +39-081-7682400; fax: +39-081-7682-404.

1359-835X/$ - see front matter © 2003 Elsevier Ltd. All rights reserved.
doi:10.1016/j.compositesa.2003.11.003

impact have not been fully explored, and are not well known presently.

In this work, the results of low-velocity impact tests carried out on a particular type of FML are presented and discussed. The material treated, labelled as 'fibreglass–aluminium' (FGA) hereafter, was very similar to GLARE®, being made of 2024 T3 sheets and S2-glass/epoxy prepreg layers. For comparison, similar tests were performed on monolithic 2024 T3 aluminium alloy panels. The thickness of the latter was calculated as the strength equivalent of the FGA for pressurised vessels application.

The analysis of the overall force–displacement ($F-d$) curves revealed that the FGA response is insensitive to the impactor mass and speed, with the $F-d$ curve only depending on the impact energy. The penetration energy was higher for monolithic aluminium than for FGA. However, the data obtained seem to indicate that the shielding ability of FGA is better compared to both CFRPs and glass fibre-reinforced plastics (GFRPs).

The progression of failure modes and their dependence on impact energy was ascertained by ultrasonic C-scan and direct observation after chemical grinding of the aluminium sheets. Matrix failures, consisting of intralaminar cracks and delamination, and plastic deformation of aluminium were found even under the lowest energy level adopted. The first fibre failure was induced by an impact energy slightly lower than that resulting in visible aluminium cracking. All these damage modes were hardly discernible from the observation of the $F-d$ curve.

Finally, the results collected were employed to obtain empirical laws correlating the maximum contact force and displacement, energy, and residual displacement.

2. Materials and test methods

The FGA tested in this work was fabricated at Alenia Aerospace, Pomigliano d'Arco, using 2024 T3 aluminium alloy sheets 0.26 mm in thickness and FM94 S2-glass/epoxy prepreg tape 0.125 mm in thickness by Cytec-Fiberite. The resin content in the prepreg was 27% by weight.

Before lay-up, the surfaces of aluminium sheets to be bonded were etched and sprayed with Cytec BR-127 primer, to improve bonding with fibreglass. Then, three rectangular flat panels of 1150 mm × 850 mm in-plane dimensions were fabricated by hand lay-up of the layers according to the stacking sequence chosen, i.e. [A/0/90/A/90/0/A]. In the laminate designation, A indicates aluminium, whereas the numbers between slashes denote the orientations of the fibreglass layers with respect to the rolling direction of metal. The cure cycle was accomplished under vacuum in autoclave, holding the material for 1 h at 121 °C temperature and 0.7 MPa pressure. The measured thickness of the cured laminate was 1.35 mm.

After fabrication, square specimens 150 mm in side were cut from each panel and ultrasonically inspected in through-transmission C-scan, to assess their integrity. Then, the samples were subjected to low-velocity impact tests using a CEAST modular falling weight machine type MK3, equipped with a DAS 4000 data acquisition system.

The impact tests were performed clamping the specimens within two steel frames having a square opening 100 mm in side, and striking them at the centre by a hemispherical impactor 15 mm in diameter. Immediately after impact, the tup was caught by a pneumatic clamp, to avoid rebound.

Two types of tests were carried out: (a) holding the impact energy constant, and suitably varying the falling height and mass; (b) fixing the impactor mass, and increasing the impact energy by increasing the falling height.

The scope of the constant energy tests was to ascertain whether the material response is affected by the impact speed or mass. To this aim, the penetration energy was measured by preliminary tests; then, an energy level U conceivably sufficient to result in complete penetration was selected ($U = 44$ J); finally, masses in the range 3.5–10.2 kg were used, and the falling height was set in such a way to fulfil the constancy of impact energy.

In the tests at increasing energy, whose main scope was the study of the failure modes, the tup mass m was 2.1 kg, and the energy was varied in the range 2.9–39 J.

In all the impact tests, each specimen was subjected to a single impact event.

The impacted samples were visually inspected, to observe eventual external damage. In the fear that hair-like microfailures could not be detected by naked eye, also liquid dye penetrant analysis was utilised. The residual displacement was measured by a micrometric dial gauge. After that, each sample was inspected anew by through-transmission ultrasonic C-scan. Then, the external aluminium sheets were chemically ground, and the internal damage was ascertained by both visual inspection and optical microscopic observation at low magnification.

Since one of the possible applications of FGA is in the fuselage of pressurised aeroplanes, where this material is a candidate substitute to aluminium alloys, a limited number of impact tests was also performed for comparison purposes on plates of monolithic 2024 T3 alloy 1.6 mm in thickness. This thickness value was calculated as the equivalent of the FGA in terms of strength for a vessel subjected to internal pressure. The tests on the aluminium alloy were carried out at increasing levels of energy, following the procedure specified previously for FGA. As will be illustrated in the discussion of the results, the energy absorption capacity of the monolithic aluminium exceeded the capabilities of the impact machine, so that no penetration was achieved. Nevertheless, the results obtained were useful to compare the performances of FGA and aluminium alloy.

3. Results and discussion

3.1. Force–displacement curves and penetration energy

A typical $F-d$ curve recorded in an impact test up to penetration on FGA is shown in Fig. 1(a). For comparison, Fig. 1(b) shows the $F-d$ curve of a GFRP [10].

A quantitative comparison of the two curves in Fig. 1 is not possible, because they were obtained on laminates of different thicknesses, using different impactor diameters and constraint conditions. However, for the present scopes, some features characterising the dynamic response of the two materials can be highlighted.

In the GFRP (Fig. 1(b)), the initial elastic phase is interrupted by an abrupt drop in the contact force, followed by similar phenomena occurring at increasing load, until the maximum force is reached. Beyond the point of maximum force, although the load continues to undergo considerable oscillations with increasing the displacement, the $F-d$ curve approaches the point of penetration (zero load) quite smoothly. The correlation between this macroscopic behaviour and the microscopic failure modes developing in the material structure has been well documented in the literature [11,12]: the first load drop is due to delamination propagation, whereas a major damage in the reinforcement is induced around the maximum load. The progressive decrease in load beyond the maximum is mainly associated with the perforation and penetration processes of the tup in the target. Of course, from the curve in Fig. 1(b), the phenomena of fibre failure, perforation, and penetration strongly contribute to the energy absorption capacity of the material.

The scheme previously depicted is hardly applicable to the FGA laminate (Fig. 1(a)). Apart low-frequency oscillations, mainly deriving from dynamic phenomena, the initial part of the $F-d$ curve does not exhibit any sudden load drop. Rather, the tangent rigidity of the specimen steadily increases with increasing the load. Only when the contact force is 80–90% of the maximum force, high-frequency oscillations of limited amplitude, suggesting possible failures in the material, are often appreciated in the $F-d$ trend (point A in Fig. 1(a)). Finally, beyond the maximum load the force rapidly falls to a value very near to zero, indicating that a negligible amount of energy is required for penetration.

In reporting the results of impact tests carried out on 2024 T3 aluminium alloy and FGA laminates, Vlot and co-workers [8,9] noted that both the materials are sensitive to the strain rate, showing an improved energy absorbing capacity with increasing the loading speed. However, this effect was much more evident for FGA than for aluminium, and FGA laminates with increasing layers of fibreglass showed more pronounced strain-rate sensitivity. The authors concluded that the strain-rate sensitivity in FGA could be mainly attributed to glass/epoxy layers, whose behaviour is typically affected by the loading speed [13,14].

In Fig. 2, two $F-d$ curves recorded during the tests carried out at constant energy, but varying the impactor mass, m, and speed, v, are shown (continuous lines). Apart minor differences, anticipated from the scatter usually affecting impact tests, the overall trend in the two cases

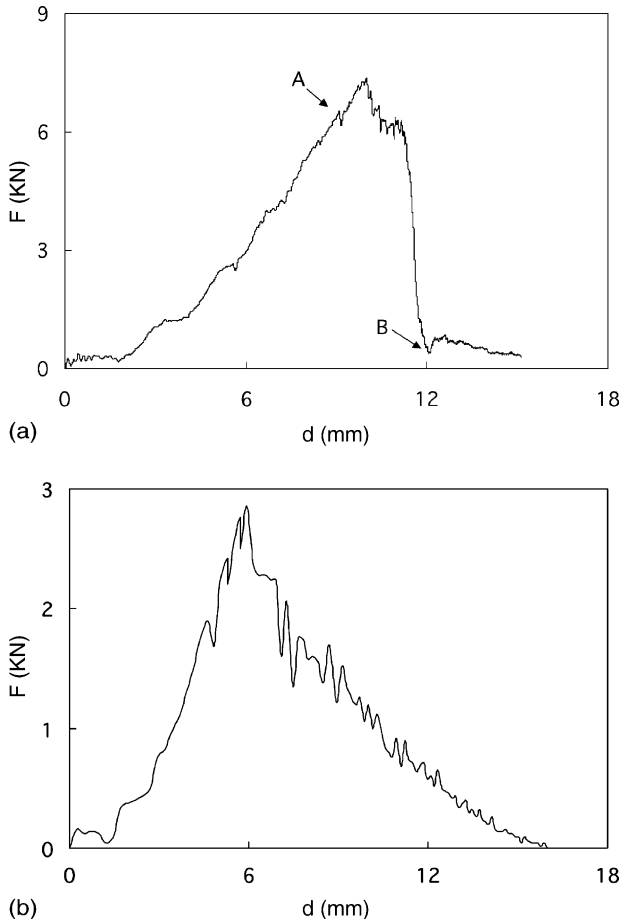

Fig. 1. Typical force–displacement curve recorded in a low-velocity impact test up to failure on: (a) the FGA tested in this work; (b) a glass fibre-reinforced plastic laminate [10].

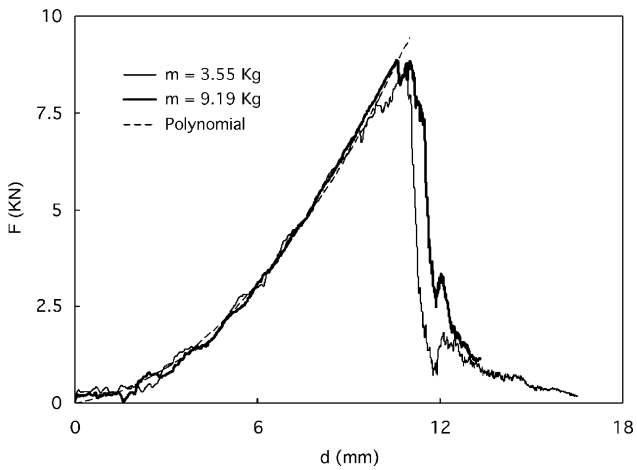

Fig. 2. Effect of the impactor mass and speed on the force–displacement curve of the FGA. Impact energy $U = 44$ J.

presented is practically the same. This result (strengthened by the analysis of all the experimental curves obtained from the constant energy tests, not reported in Fig. 2 to avoid crowding of data) supports the statement that, within the range of m and v values considered, the energy, rather than mass and speed separately, influences the macroscopic material response. Although this finding may appear in contrast with the conclusions drawn by Vlot and et al. it must be recalled that in Refs. [8,9] the projectile speed was approximately varied in the range 10–100 m/s, whereas in this work the maximum speed was only 70% higher than the minimum one.

The dashed curve in Fig. 2 is the graphical representation of the polynomial law of equation:

$$F = ad^2 + bd \tag{1}$$

where the constants a and b were calculated by the best fit method, obtaining $a = 0.069\ \text{kN/mm}^2$ and $b = 0.10\ \text{kN/mm}$. In applying the best-fit procedure, the part of the $F–d$ curve beyond the point A in Fig. 1(a) was disregarded. The actual trend of the $F–d$ curves is very well shaped by the polynomial curve. However, after the first evident load drop has occurred, a divergence of the real curve from Eq. (1) is clearly noted. This behaviour supports the hypothesis that some major failure phenomenon is associated with point A in Fig. 1(a).

The penetration energy U_p was evaluated as the area under the $F–d$ curves resulting from the tests at constant energy. U_p was conventionally measured in correspondence of the point B in Fig. 1(a). This allowed for the easy individuation of a reference point on all the experimental curves.

Fig. 3 shows the penetration energy as a function of the impactor mass. As expected from Fig. 2, also U_p is independent of the mass and velocity. The dashed horizontal straight line in the figure is the mean value of the penetration energy, which was found to be 39.7 J.

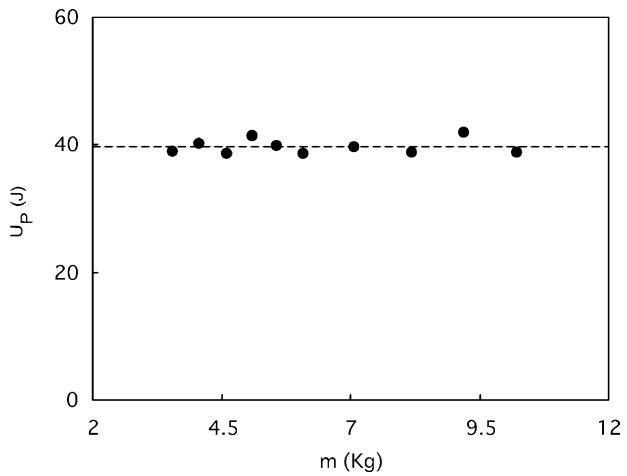

Fig. 3. Penetration energy, U_p, against impactor mass, m, as measured from the tests at constant energy. Impact energy $U = 44$ J.

From a practical viewpoint, it is interesting to wonder whether substituting an FGA to a conventional FRP results in an improvement in the shielding ability of an aeronautical component. A direct answer to this question could not be given from the tests carried out in this work, where no GFRP or CFRP composites were characterised. Nevertheless, some considerations on this topic can be desumed from the empirical relationship:

$$U_p = K(tV_fD_t)^{\alpha} \tag{2}$$

proposed in Ref. [15] for an approximate calculation of the penetration energy of composite laminates under low velocity impact. In Eq. (2), K and α are two constants, depending on the reinforcing fibres, but independent of their architecture, matrix type and constraint conditions; further, t is the laminate thickness, V_f the fibre volume fraction, and D_t the tup diameter.

The values of the constants K and α found in Ref. [15] were $K = 0.49\ \text{J/mm}^{2\alpha}$ and $\alpha = 1.40$ for CFRP, and $K = 0.90\ \text{J/mm}^{2\alpha}$ and $\alpha = 1.30$ for GFRP. With these values, and assuming for the composite the same thickness of the FGA examined here ($t = 1.35$ mm) and $V_f = 0.6$, the penetration energy for CFRP is 16.2 J, and for GFRP 23.1 J, sensibly lower than the value measured for the FGA. Of course, the comparison can be also carried out on the basis of the same areal weight, which would imply the same structural weight. In this case, considering that the areal weight of the FGA is $3.2\ \text{kg/m}^2$, the equivalent thicknesses for GFRP and CFRP are approximately calculated as 1.6 and 2.0 mm, respectively, and the associated penetration energies are about 28 J for both the FRPs. Therefore, the FGA seems to offer better performances, independently of the fact that the comparison is carried out fixing the thickness or the areal weight.

Fig. 4 compares the force–displacement curves of the FGA and 2024 T3 aluminium alloy. As specified in Section 2, the 2024 T3 panels were thicker ($t = 1.60$ mm), and therefore considerably heavier ($4.4\ \text{kg/m}^2$) than FGA, because the equivalence was established on the basis of

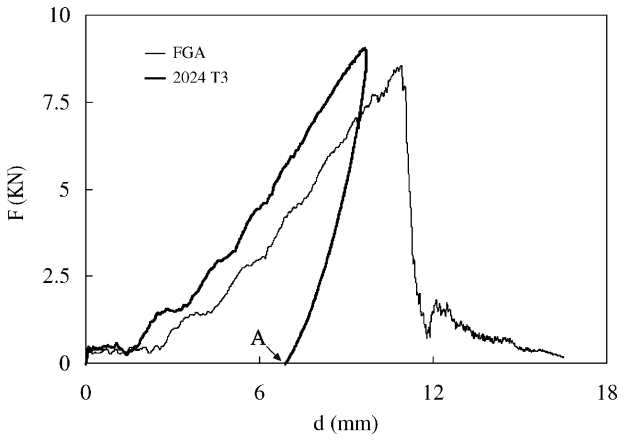

Fig. 4. Force–displacement curves for 2024 T3 aluminium alloy and FGA.

the same safety factor, should the materials be used for the shell of a pressure vessel. The difference in thickness mainly explains the higher rigidity of the aluminium alloy, whose $F-d$ curve in Fig. 4 refers to an impact energy $U = 36$ J. This energy level was unable to induce penetration in aluminium, as desumed from the unloading portion of the curve after the achievement of the maximum displacement. Unfortunately, it was impossible to record the complete impact curves of the aluminium alloy beyond $U = 36$ J, because this resulted in the saturation of the force measuring instrumentation. However, non-instrumented impact tests were carried out up to 44 J, without generating any penetration or material cracking. It is concluded that the 2024 T3 alloy offers a better protection against penetration than FGA, if the safety factor is assumed as a basis for comparison. Of course, this advantage also involves a $\approx 30\%$ increase in structural weight.

3.2. Relevant impact parameters

Fig. 5 shows the maximum contact force experienced during impact, F_{max}, against the impact energy, U. The open and black symbols refer to FGA and monolithic aluminium alloy, respectively.

At low energy, there is negligible difference in the response of the two materials. A divergence is observed only at high energies, where the maximum force carried by FGA approaches or equals the panel failure load (maximum force value in Figs. 1(a) and 2).

Considering that the impact energy, force, and displacement are linked by the well-known equation:

$$U = \int_0^d F \, \mathrm{d}(d) \tag{3}$$

and accounting for Eq. (1), the following relationship is obtained immediately:

$$U = \frac{ad^3}{3} + \frac{bd^2}{2} \tag{4}$$

which provides the energy corresponding to a given displacement.

Of course, using Eqs. (1) and (4), the correlation between U and the maximum force for the FGA can be calculated. The result is represented by the continuous curve in Fig. 5. The agreement between the theoretical prediction and the experimental points is excellent up to about 20 J, which approximately corresponds to the point A in Fig. 1(a). Beyond this energy value, the theoretical curve overestimates the actual maximum force, as expected from the progressive departure of Eq. (1) from the experimental $F-d$ curve (Fig. 2).

For a given impact energy, the maximum displacement d_{max} sustained by the FGA is slightly higher than that suffered by aluminium (Fig. 6). For both the materials, the rate of increase in d_{max} considerably lowers as higher energies are concerned, conceivably because of the membrane effects, which manifest themselves at large displacements. The solid line in Fig. 6 is the graphical representation of Eq. (4): it is seen that, even at high energies, the accuracy of the theoretical curve is quite good.

It is well known that, when an impact test is carried out using an energy lower than the penetration energy, the unloading portion of the $F-d$ curve is separated from the loading portion (see for instance Fig. 4). The area enclosed in the loading–unloading curve is the energy U_d dissipated by vibrations, plastic deformation, and damage formation. In Fig. 7, U_d is shown against the impact energy, U, for the two materials tested. Up to 20–22 J, the variation of the dissipated energy as a function of U is well represented by a straight line; roughly speaking, 60% of the impact energy is not restituted to the tup in this domain, irrespective of the material considered. Beyond about 22 J, an evident deviation from linearity is observed for the FGA, with the ratio U_d/U steadily approaching unity as the penetration energy is approached. Together with the observations made in commenting Fig. 2, this behaviour strengthens the conjecture that a major damage occurs in the material when a 20 J impact energy or higher is imparted. Also

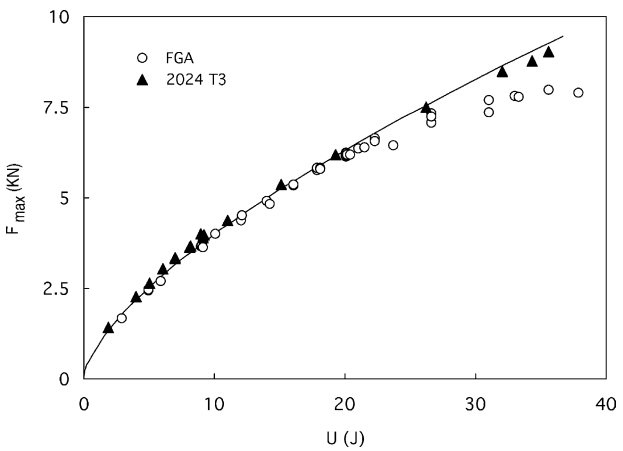

Fig. 5. Maximum contact force, F_{max}, against impact energy, U.

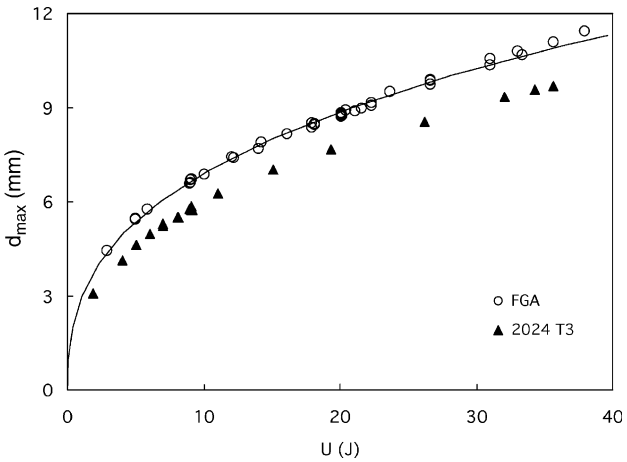

Fig. 6. Maximum displacement, d_{max}, against impact energy, U.

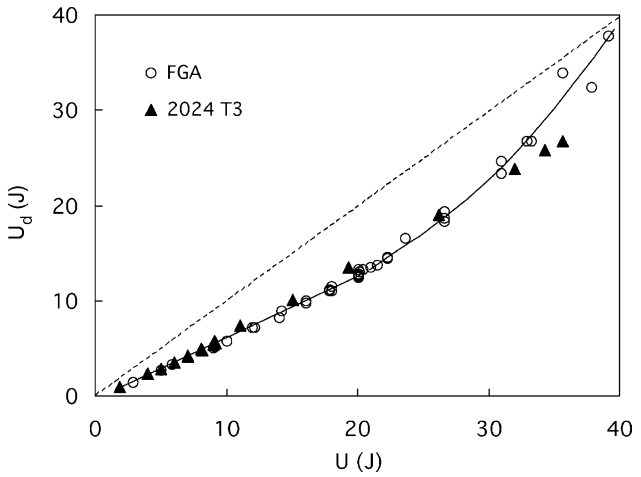

Fig. 7. Dissipated energy, U_d, against impact energy, U.

the monolithic aluminium alloy undergoes a perceivable, although less distinct departure from linearity at high energies.

3.3. Impact damage

The damage the FGA undergoes as a consequence of impact was characterised by visual inspection, non-destructive ultrasonic C-scan, and destructive analysis. The results obtained are discussed in this section.

The scopes of the visual inspection were: (a) the evaluation of the permanent deformation, and, (b) the detection of possible cracks emerging on the surfaces of the panels.

To resort to a quantitative estimate of the permanent deformation, the residual displacement d_r of the specimens was measured. The label 'residual displacement', instead of the more common term 'indentation depth' is used here, because of the peculiar behaviour of FGA compared to a common FRP. In fact, due to the plasticity of aluminium, the permanent deformation was not limited to a little zone surrounding the impact location. Rather, only the portion of the specimen boundaries clamped within the test frame was unaltered at the end of the impact event, whereas the rest of the plate exhibited a pronounced concavity (Fig. 8). Of course, this impaired the possibility to easily separate the indentation depth (usually correlated with the local damage) from the overall residual displacement.

Fig. 9 clarifies the meaning of the residual displacement, as conventionally defined in this work. Of course, according to this definition, the actual value of d_r is presumably very much dependent on the panel dimensions, increasing with increasing the latter.

The measurement of d_r was carried out immediately after each impact test, holding the specimen in the test frame of the impact machine. Two different methods were used: (a) the tup was put in contact with the indented panel, and its vertical displacement with respect to the reference plane of

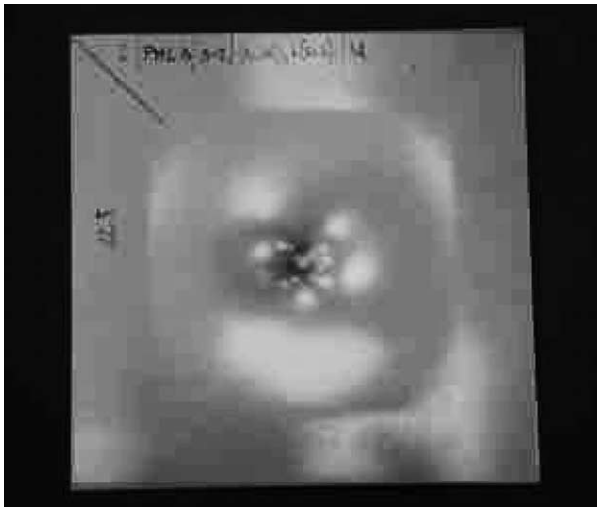

Fig. 8. Permanent deformation of an FGA specimen after impact.

the integer specimen was measured; (b) d_r was directly measured by using a micrometric dial gauge with a hemispherical tip 2 mm in diameter. The results obtained were substantially the same for the two methods. In the following discussion, reference will be made only to the procedure specified in (b).

The dependence of d_r on the impact energy for FGA is shown in Fig. 10 (open symbols). The continuous curve, drawn by hand, evidences the trend of the experimental data.

Of course, the residual displacement is larger for higher U values; however, its rate of increase clearly decreases with increasing U, probably because of the plate stretching effects becoming more and more effective when the large displacement regime is reached. Notably, the residual displacement values attained before penetration are sensibly larger than the dent depth in an FRP laminate. Further, an easily visible residual deformation is present even when the impact energy is particularly low. From the latter features, FGA seems to offer easier inspectability than a typical FRP.

The black triangles in Fig. 10 refer to 2024 T3. Despite the difference in thickness between this material and FGA, the behaviour of the aluminium alloy is identical to that of FGA at sufficiently low energy levels. This probably reflects the role played by the fibreglass layers, which limit the plastic deformation of FGA. Only for energies higher than about 15 J, the residual deformation of 2024 T3 becomes slightly lower than that of FGA, for a fixed U.

In Fig. 11, the residual displacement of FGA (open circles) is plotted against the maximum contact force experienced during impact, F_{max}. The solid straight line in the figure, having equation:

$$d_r = 0.8558F_{max} - 0.1492 \quad (5)$$

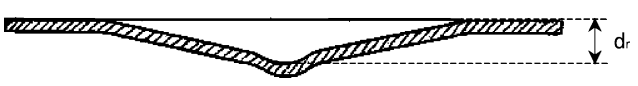

Fig. 9. Conventional definition of the residual displacement, d_r.

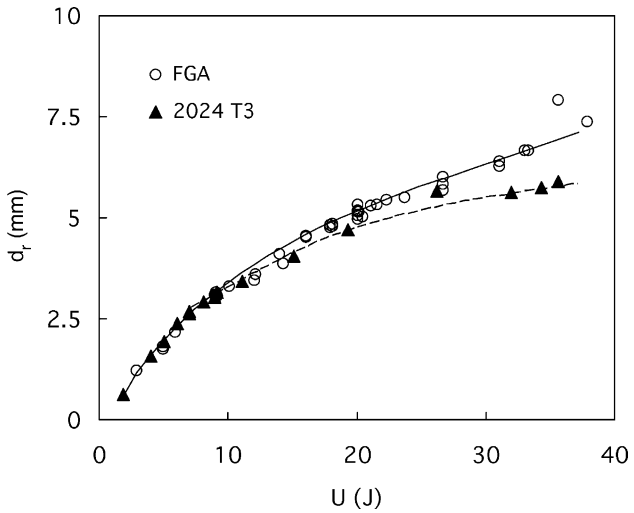

Fig. 10. Residual displacement, d_r, against impact energy, U.

was obtained by best fit, excluding the two extreme points on the right in the figure, concerning tests in which the failure load of the panel (the maximum load in Fig. 1(a) was overcome. Eq. (5) provides d_r in mm, when F_{max} is given in kN. The agreement between the best-fit straight line and the experimental points in Fig. 11 is excellent, as appears also from the coefficient of correlation, $R^2 = 0.993$.

The black triangles in Fig. 11 concern the monolithic aluminium. The behaviour of this material is only negligibly different from that of FGA, except when the contact force is very high. In this domain, the residual displacement of 2024 T3 tends to level off, despite the increase in F_{max}.

Also the correlation between the maximum displacement the panel undergoes during impact, d_{max}, and d_r obeys a simple, linear relationship for both FGA and aluminium alloy (Fig. 12). The two best-fit straight lines, drawn in Fig. 12, have coincident slope; however, for a given d_{max}, the FGA retains a smaller portion of the overall displacement under form of residual deformation, presumably thanks to the presence of fibreglass.

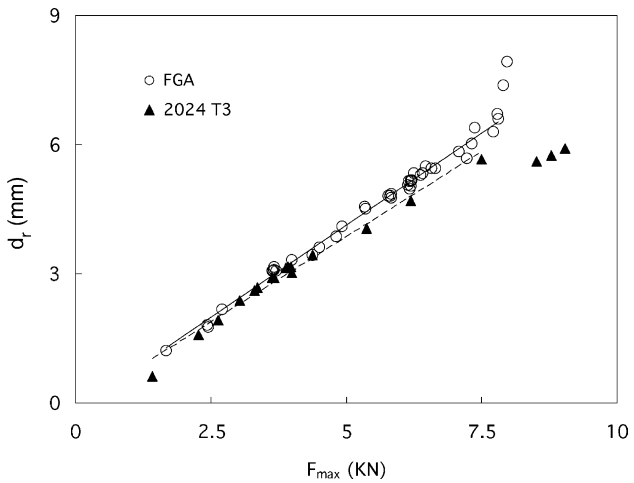

Fig. 11. Residual displacement, d_r, against maximum contact force, F_{max}.

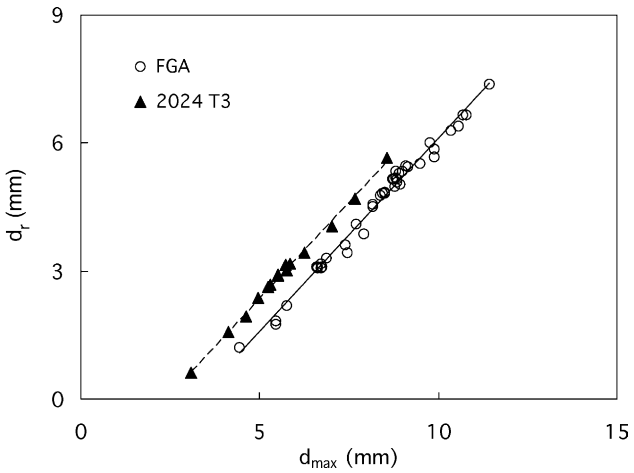

Fig. 12. Residual displacement, d_r, against maximum displacement suffered during impact, d_{max}.

From the best-fit straight line (solid line in Fig. 12), the following equation was found for FGA:

$$d_r = 0.9034 d_{max} - 2.9323 \quad (6)$$

where d_r is given in mm for d_{max} in mm. Also in this case, the coefficient of correlation was very near to unity ($R^2 = 0.987$).

It must be recognised that Eqs. (5) and (6) are empirical in nature, and their validity only holds within the ranges of abscissa values covered by the experimental data in Figs. 11 and 12. Forgetting this basic concept may bring to mistakes in the interpretation of the results. For instance, one could interpret the intercept of the continuous line in Fig. 12 with the x-axis ($d_{max} = d_{maxo} = 3.25$ mm) as the limit displacement beyond which no residual displacement is verified.

Using Eq. (4) for $d = d_{maxo}$, the value $U = U_0 = 1.32$ J, which could be considered as the limit energy for the first plastic deformation of the panel, is recovered. On the other hand, combining Eqs. (5) and (6), the relationship:

$$d_{max} = 0.9473 F_{max} + 3.081 \quad (7)$$

clearly in contrast with Eq. (1), is obtained. It is easily seen that Eq. (7) does not fulfil the boundary condition $d_{max} = 0 \Rightarrow F_{max} = 0$, and therefore is particularly inaccurate at low displacements and forces.

Although the previous discussion highlights that a reliable estimate of U_0 is impossible from the data generated here, the trend of the experimental results in Fig. 10 suggests that, under the test conditions adopted, very low energy levels can actually result in a permanent displacement of the plate.

In principle, it can be thought that there is no need to measure the residual displacement, because this quantity should be directly provided by the intersection of the unloading part of the $F-d$ curve with the x-axis (see for example point A in Fig. 4). In Fig. 13, the residual displacement measured according to this procedure, indicated by the symbol d_r^*, is compared with d_r. The dashed

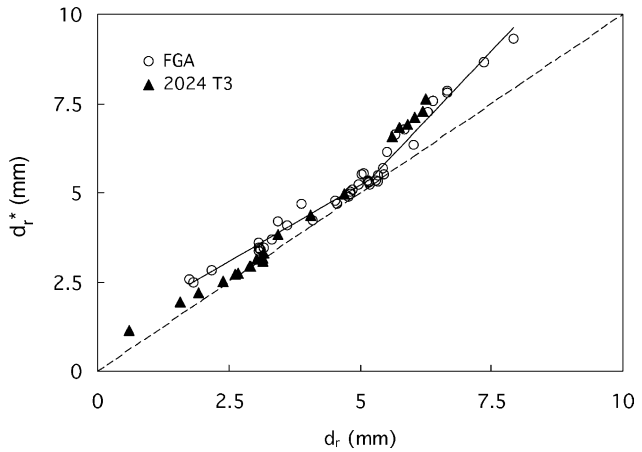

Fig. 13. Residual displacement measured after test, d_r, against residual displacement evaluated through the force–displacement curve, d_r^*.

straight line, drawn as a reference, represents the points satisfying the condition $d_r^* = d_r$.

It is seen that all the points in Fig. 13 fall in the domain $d_r^* \geq d_r$. Therefore, assuming d_r^* instead of d_r as a measurement of residual displacement generally results in an overestimate of the actual plastic deformation for both FGA and monolithic aluminium. However, the error made for 2024 T3 at low d_r values is lower than that pertaining to FGA. Interestingly, in the case of FGA a knee is noted in the trend of the experimental data, as the two continuous straight lines drawn in the figure evidence. In correspondence of the knee, d_r^* and d_r practically coincide.

As specified previously, in the visual inspection of the panels after impact the liquid dye penetrant technique was used, to help detect possible microcracks on the aluminium surfaces. The tests carried out revealed that, when a crack is generated in an aluminium sheet, it propagates in an unstable manner, achieving a length easily visible by naked eye. Therefore, the non-destructive evaluation through liquid dye penetrant was no longer utilised in subsequent analyses.

No cracks were found in the monolithic aluminium alloy, even under the most severe impact conditions ($U = 44$ J).

The first external crack in FGA, oriented along the rolling direction, was found in the aluminium sheet far from the impact surface, at energy of about 20 J (Fig. 14(a)). As previously noted, this energy level approximately coincides with the load drop indicated by 'A' in Fig. 1(a). However,

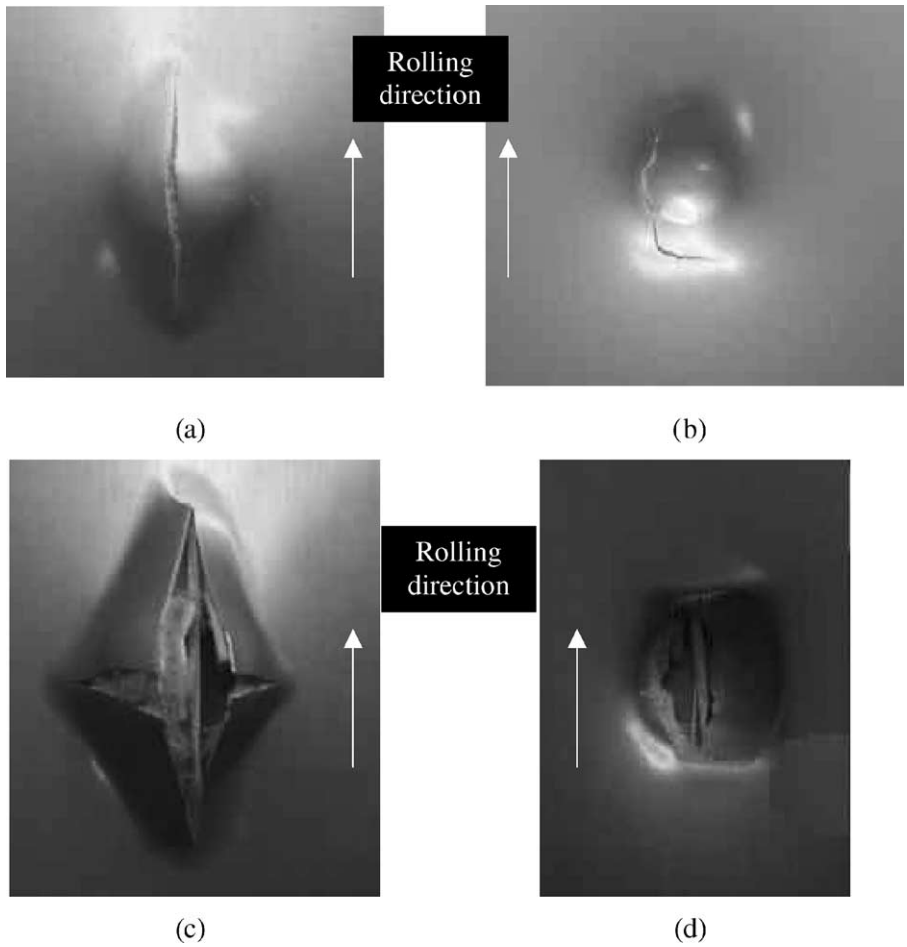

Fig. 14. External damage in the aluminium layers of FGA: (a) non-impacted side, $U = 20$ J; (b) impacted side, $U = 33$ J; (c) non-impacted side, penetrated and (d) impacted side, penetrated.

the abrupt load decrease is probably not directly associated with the crack nucleation, because in some cases the first aluminium cracking was detected without any load drop in the $F-d$ curve.

From Fig. 10, $U = 20$ J corresponds to $d_r \approx 5$ mm, which compares well with the location of the knee point noted in Fig. 13, and with the departure from linearity of the curve in Fig. 7. It is quite surprising that, although this major failure phenomenon seems to affect the law of variation of dissipated energy (Fig. 7) and the correlation between d_r^* and d_r (Fig. 13), no sign of its occurrence is clearly visible in the diagrams in Figs. 5, 6, 10, 11, and 12, and even in the force–displacement curve.

In Ref. [9], where impact tests were carried out on GLARE® panels using the same test conditions adopted in this work, the energy required for first aluminium cracking was found to increase with increasing the material thickness. In particular, the minimum cracking energy was 21.4 and 26.2 J for 0.85 and 1.4 mm thicknesses, respectively. The value found here seems to be lower than that measured in Ref. [9], despite the fact that the first visible failure mode was the same.

For $U = 36-38$ J, also the aluminium sheet directly struck by the impactor is cracked (Fig. 14(b)). The crack forms just outside the material-tup contact zone, as typically occurs for monolithic aluminium loaded by a hemispherical impactor.

When the impact energy is sufficient to provoke penetration ($U_p \approx 39$ J), a new crack, perpendicular to the rolling direction, appears in the metal sheet at the back side of the panel (Fig. 14(c)), whereas the crack in the front sheet propagates along the periphery of the contact zone (Fig. 14(d)).

The ultrasonic C-scan analysis of the impacted specimens evidenced some internal damage even for the lowest impact energy level adopted ($U = 2.9$ J, Fig. 15(a)). The arrow in Fig. 15(a) indicates the impact point location, whereas the black area on the right of the impact point was drawn for calibration purposes. Comparing Fig. 15(a) with (b), where the map of a specimen loaded at higher energy is shown, the damage is initially approximately circular, whereas it tends to assume an ellipsoidal shape in growing more and more. The major axis of the ellipsoid is oriented parallel to the rolling direction of aluminium. It is important to note that this direction also coincides with the orientation of some of the fibreglass layers. Consequently, it cannot be easily desumed whether the preferential propagation of damage is driven by the anisotropy of aluminium, GFRP, or both.

The extent of the damaged area, as revealed by the ultrasonic analysis, is plotted in Fig. 16 (open triangles) against the impact energy. Similarly to Fig. 13, a bilinear trend is found, with the knee roughly corresponding to the energy level resulting in the first cracking in aluminium. Notably, the first segment of the bilinear curve (low energy) tends to pass through the origin of the coordinate axes, suggesting, in agreement with the data in Fig. 10 discussed previously, that the energy for first damage is very low.

Undoubtedly, there are some difficulties in using the ultrasonic method to non-destructively evaluate the damage extent of an FGA. In fact, the acoustic impedance of the two materials coupled (fibreglass and aluminium alloy) is very different, rendering hard an accurate analysis of the failure modes. In addition, the considerable plastic deformation of the panel may provide a distorted map of the actual situation, especially in correspondence of the impact point. Therefore, to gain better insight into the failure phenomena occurring in the FGA, the external aluminium sheets were chemically ground. Unfortunately, this method only allowed the examination of fibreglass layers by optical microscopy at low magnification, whereas possible debonding between them and metal could not be ascertained. The main information provided by C-scan was qualitatively confirmed. However, additional knowledge was gathered on the mechanisms of damage type and progression, as will be illustrated in the following.

When the minimum impact energy ($U = 2.9$ J) is adopted, the damage in the fibreglass layers essentially consists of intralaminar matrix cracking and delamination. The damage extent, easily detectable from the withening of

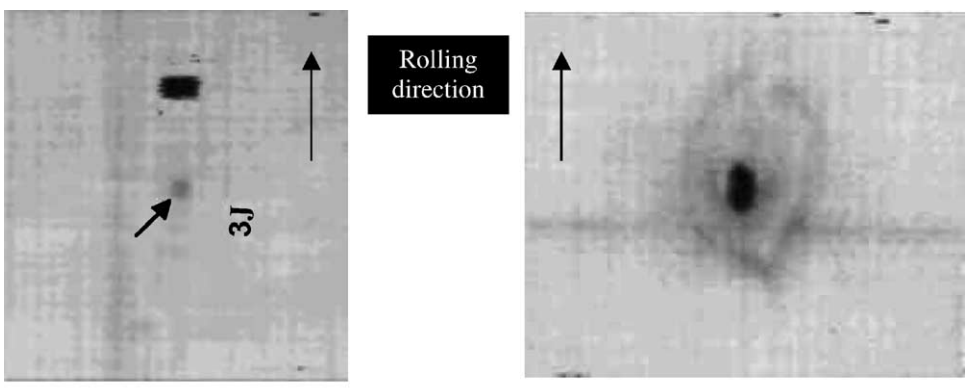

Fig. 15. Ultrasonic C-scan of impacted FGA panels: (a) $U = 3$ J and (b) $U = 12$ J.

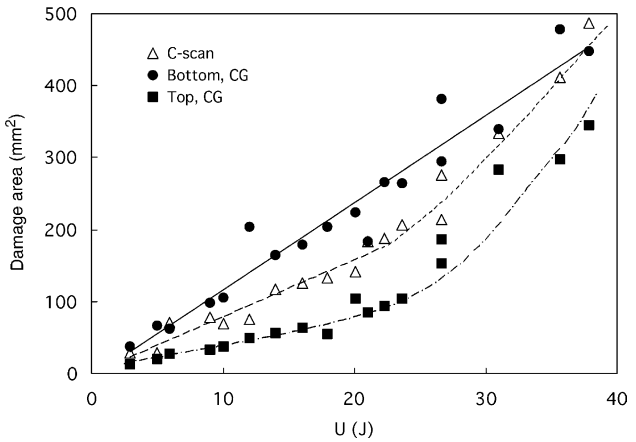

Fig. 16. Damage area detected by different methods against impact energy, U.

the composite, is sensibly larger in the layers far from the impact side (Fig. 17(a)) than in those near to it (Fig. 17(b)). This characteristic is shared with typical FRP laminates, often exhibiting the so-called 'hat-shaped' distribution of damage along the thickness direction [3,16]. Further, the microscopic analysis reveals the ellipsoidal nature of delamination even under this low impact threat.

Fig. 16 (black points) shows the effect of the impact energy on the damaged area, evaluated after chemical grinding, in the composite layers near to (Top, CG) and far from (Bottom, CG) the impact surface. In both the blocks of fibreglass, the damage extent increases initially according to a linear law. The rate of increase is higher at the bottom, so that the difference between the two areas increases progressively. However, while the same linear variation is preserved up to penetration for the bottom layers, a progressive shift through a different linear law, of higher slope, is found for the top layers beyond about 20 J.

Comparing the damaged areas obtained by C-scan with those detected after chemical grinding, the former seem to somehow provide a 'mean value' of the actual damage extent. This only indicates that additional work is required, in order to achieve a more effective non-destructive evaluation of FGA through ultrasonic inspection.

If the maximum damaged area in Fig. 16 is considered (about 500 mm^2), the corresponding equivalent diameter (i.e. the diameter of the circle having the same area) is approximately 25 mm, less than two times the impactor diameter. This datum highlights the excellent damage resistance of FGA: larger equivalent diameters have been reported in the literature for typical FRP laminates [17,18], and even for stitched composites [3,19], impacted under energy levels far lower than their penetration energy.

The first glass fibre failure occurs for $U \approx 18$ J, and concerns the reinforcement of the two layers far from the front side of the panel. Evidently, the energy levels required for fibre damage in each single layer are very near or coincident, because in no case fibre failure in one layer was found, the reinforcement being intact in the other layer. The failure in each layer is located beneath the initial tup-material contact point, and extends perpendicularly to the fibre orientation (see arrow in Fig. 18), as is also guessed from the images collected after penetration (Fig. 14(c)).

In the energy range 26–30 J many failure events occur, concerning the fibres in the two GFRP layers near to the contact surface, and the central aluminium sheet. The first layer to show reinforcement failure is that adjacent to the central aluminium sheet, oriented at 90° with respect to the rolling direction. The failure path crosses the fibre bundles at some distance from the impact point (Fig. 19(a)). Seemingly, this event induces rare fibre breaking in the GFRP layer nearest to the impact surface, and cracking in the aluminium sheet at the centre of the laminate. The crack in aluminium is initially oriented along the rolling direction (Fig. 19(b)), and substantially replicates the shape of the fibre failures in the 90° GFRP layer. Its radial distance from the vertical axis passing through the impact point is shorter than that characterising the crack in the front metal sheet. Consequently, the failures in the aluminium alloy sheets and in the glass fibres along the thickness approximately follow a conical path, which is reversed compared to the hat shaped delamination. Unfortunately, the data available did not allow

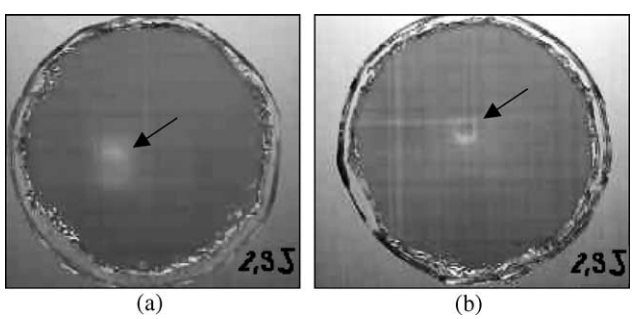

Fig. 17. Damage in an FGA panel after impact with $U = 2.9$ J: (a) rear side and (b) front side.

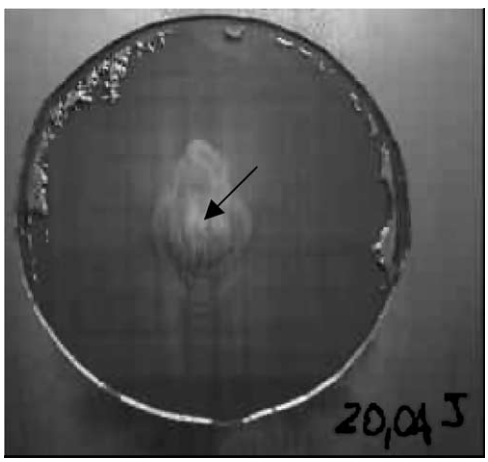

Fig. 18. Fibre failures in the composite layers far from the impact point. Energy level $U = 20$ J.

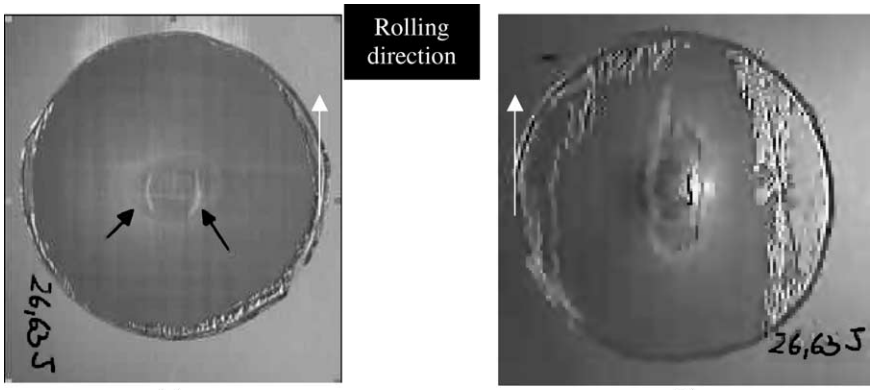

Fig. 19. (a) Fibre failure initiation in the composite layers near to the impact point, and, (b) crack in the central aluminium sheet.

the identification of the threshold energy levels resulting in each of the failure modes described.

From the observations illustrated, the sequence of damage with increasing the impact energy can be reconstructed. Its progression is briefly resumed in the following with reference to Fig. 20, from which the approximate correlation between the failure mode initiation and the $F-d$ curve evolution is established:

- a delamination between both the upper and lower GFRP couples of layers occurs under an impact energy lower than 2.9 J;
- for $U \approx 18$ J, the glass fibres in the two layers farther from the front side begin to be broken (FF/B, fibre failure/back in Fig. 20);
- for $U \approx 20$ J, a crack begins to form in the metallic sheet farthest from the impacted side (AF/B, aluminium failure/bottom);
- in the energy range 26–30 J, the reinforcement failure in the two composite layers near to the impacted side (FF/F, fibre failure/front) occurs, followed by cracking of the central aluminium sheet (AF/C, aluminium failure/centre);
- for $U = 36-38$ J, the front metal sheet cracks (AF/F, aluminium failure/front);
- when the energy exceeds 39 J, penetration occurs.

Comparing Figs. 1(a) and 20, some variation in the material response, due to scatter from specimen to specimen, is noted mainly in the last part of the $F-d$ curve. Due to this, the point of maximum force could not be associated with a specific failure mode. In most of the tests analysed, F_{max} was reached when the aluminium sheet at the centre of the material was cracked; however, sometimes it corresponded to the crack formation in the front metallic sheet.

In the GLARE® material tested in Ref. [9], a failure in the glass fibres was never detected before aluminium cracking, which contrasts with the results obtained in this work. Recalling the small gap between the energy levels resulting in these damage modes in the FGA, this disagreement is probably attributable to the differences between FGA and GLARE®.

4. Conclusions

From the results illustrated in this work, where low-velocity impact tests were carried out on a fibreglass–aluminium (FGA) laminate, the main conclusions are as follows.

- The material displays the same force–displacement curve for a given energy level, independently on the tup mass and speed. This statement holds within the limits of the speed values adopted here, where the maximum impactor speed was about 70% higher than the minimum one.
- From the force–displacement curve, the failures occurring in the material cannot be easily inferred. In fact, considerable damage is accumulated in the FGA, before a clear evidence of it is visible in the trend of the contact

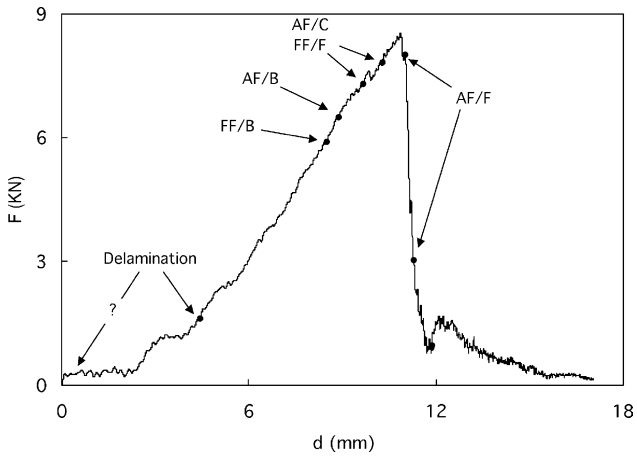

Fig. 20. Correspondence between the force–displacement curve and the failure modes initiation.

force. Some relevant impact parameters, as the dissipated energy and the residual displacement, appear to be more sensitive than the $F-d$ curve to the main failure initiation phenomena.

- The response of FGA to complete penetration seems to be better than that of carbon fibre- and GFRPs. However, a monolithic aluminium alloy of equivalent thickness is more effective than FGA in preventing penetration.
- The plastic behaviour of aluminium layers results in an easily visible residual displacement, rendering the FGA particularly suitable to inspection operations. Further, the FGA exhibits an excellent impact damage resistance, showing a small damaged area even at complete penetration. Unfortunately, the energy level determining first damage (consisting of delamination between the composite layers and aluminium sheet plasticisation) is very low.
- The correlation between the relevant impact parameters (maximum force and displacement, residual displacement, and energy) can be described by simple empirical laws, provided the material is far enough from penetration.

Acknowledgements

This work was partially supported under the Program 'Non-destructive evaluation of structural composite materials for aeronautics' by MIUR (Italian Ministry for Industry, University and Research).

References

[1] Chestney JA, Sarhadi M. Control and integration techniques in a fully automated manufacturing cell for carbon composites. IEE Proc—Control Theory Appl 1996;143:159–63.
[2] Groppe D. Robotic 'layup' of composite materials. Assembly Autom 2003;23:153–8.
[3] Bibo GA, Hogg PJ, Backhouse R, Mills A. Carbon-fibre non-crimp fabric laminates for cost-effective damage-tolerant structures. Compos Sci Technol 1998;58:129–43.
[4] Greenhalgh E, Hiley M. The assessment of novel materials and processes for the impact tolerant design of stiffened composite aerospace structures. Compos Part A 2003;34:151–61.
[5] Vogelesang LB, Vlot A. Development of fibre metal laminates for advanced aerospace structures. J Mater Process Technol 2000; 103:1–5.
[6] Young JB, Landry JGN, Cavoulacos VN. Crack growth and residual strength characteristics of two grades of glass-reinforced aluminium GLARE. Compos Struct 1994;27:457–69.
[7] Papakyriacou M, Schijve J, StanzlTschegg SE. Fatigue crack growth behaviour of fibre–metal laminate GLARE-1 and metal laminate 7475 with different blunt notches. Fatigue Fract Engng Mater Struct 1997;20:1573–84.
[8] Vlot A. Impact loading on fibre metal laminates. Int J Impact Engng 1996;18(3):291–307.
[9] Vlot A, Krull M. Impact damage resistance of various fibre metal laminates. J. de Physique IV 1997;7(C3):1045–50.
[10] Caprino G. Unpublished data.
[11] Caprino G, Lopresto V. Factors affecting the penetration energy of glass fibre reinforced plastics subjected to a concentrated transverse load. Proc. ECCM9, Brighton, 4–7 June 2000, paper Wedn. 7, Room A, Section 'Polymer Matrix Composites—Impact and Fracture'; 2000.
[12] Kim J-K, Sham M-L, Sohn M-S, Hamada H. Effect of hybrid layers with different silane coupling agents on impact response of glass fabric reinforced vinylester matrix composites. Polymer 2001;42: 7455–60.
[13] Harding J. Effect of strain rate and specimen geometry on the compressive strength of woven glass reinforced epoxy laminates. Composites 1993;24:323–32.
[14] Barré S, Chotard T, Benzeggagh ML. Comparative study of strain rate effects on mechanical properties of glass fibre-reinforced thermoset matrix composites. Compos Part A 1996; 27A:1169–81.
[15] Caprino G, Lopresto V. On the penetration energy of fibre reinforced plastics under low-velocity impact conditions. Compos Sci Technol 2001;61:65–73.
[16] Gao S-L, Kim J-K. Cooling rate influences in carbon fibre/PEEK composites. Part III: impact damage performance. Compos Part A 2001;32:775–85.
[17] Im K-H, Cha C-S, Kim S-K, Yang I-Y. Effects of temperature on impact damages in CFRP composite laminates. Compos Part B 2001; 32:669–82.
[18] Teti R, Buonadonna P, Lopresto V, Caprino G. Volumetric ultrasonic NDE of damaged CFRP laminates. . Proc. ECCM 10, Brugge, 3–7 June 2002, Paper n. 346.; 2002.
[19] Larsson F. Damage tolerance of a stitched carbon/epoxy laminate. Compos Part A 1997;28A:923–34.